Lateral Size-Dependent Spontaneous and Stimulated Emission Properties in Colloidal CdSe Nanoplatelets

Murat Olutas,[†,‡,#] Burak Guzelturk,[†,#] Yusuf Kelestemur,[†] Aydan Yeltik,[†] Savas Delikanli,[†] and Hilmi Volkan Demir*[,†,§]

[†]Department of Electrical and Electronics Engineering, Department of Physics, UNAM—Institute of Materials Science and Nanotechnology, Bilkent University, Ankara 06800 Turkey, [‡]Department of Physics, Abant Izzet Baysal University, Bolu 14280, Turkey, and [§]Luminous! Center of Excellence for Semiconductor Lighting and Displays, School of Electrical and Electronic Engineering, School of Physical and Mathematical Sciences, Nanyang Technological University, Nanyang Avenue, Singapore 639798, Singapore. [#]M. Olutas and B. Guzelturk contributed equally to this work.

ABSTRACT Here, we systematically investigated the spontaneous and stimulated emission performances of solution-processed atomically flat quasi-2D nanoplatelets (NPLs) as a function of their lateral size using colloidal CdSe core NPLs. We found that the photoluminescence quantum efficiency of these NPLs decreases with increasing lateral size while their photoluminescence decay rate accelerates. This strongly suggests that nonradiative channels

prevail in the NPL ensembles having extended lateral size, which is well-explained by the increasing number of the defected NPL subpopulation. In the case of stimulated emission the role of lateral size in NPLs influentially emerges both in the single- and two-photon absorption (1PA and 2PA) pumping. In the amplified spontaneous emission measurements, we uncovered that the stimulated emission thresholds of 1PA and 2PA exhibit completely opposite behavior with increasing lateral size. The NPLs with larger lateral sizes exhibited higher stimulated emission thresholds under 1PA pumping due to the dominating defected subpopulation in larger NPLs. On the other hand, surprisingly, larger NPLs remarkably revealed lower 2PA-pumped amplified spontaneous emission thresholds. This is attributed to the observation of a "giant" 2PA cross-section overwhelmingly growing with increasing lateral size and reaching record levels higher than 10^6 GM, at least an order of magnitude stronger than colloidal quantum dots and rods. These findings suggest that the lateral size control in the NPLs, which is commonly neglected, is essential to high-performance colloidal NPL optoelectronic devices in addition to the vertical monolayer control.
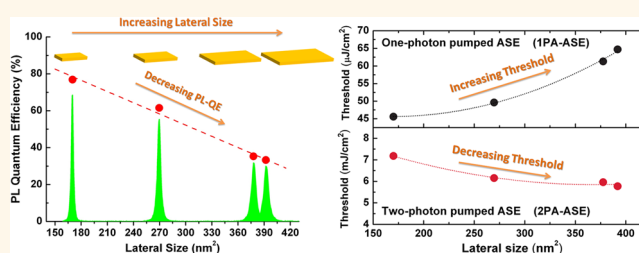
KEYWORDS: semiconductor nanoplatelets · colloidal quantum wells · lateral size · photoluminescence quantum efficiency · amplified spontaneous emission · stimulated emission · giant two-photon absorption cross-section

Since the first synthesis of colloidal semiconductor nanocrystals (NCs),[1] there is an ever-increasing interest in colloidal nanomaterials owing to their unique optical and electronic features that enable advanced optoelectronic devices.[2−6] The physical properties of the colloidal semiconductors can be engineered by tailoring their size and shape in addition to composition. There are previous reports that studied strongly size-dependent optical properties in colloidal quantum dots including extinction coefficient, photoluminescence quantum efficiency (PL-QE), and multiexciton kinetics in relation to nonradiative Auger recombination.[7−15] Recently, a new type of atomically flat nanocrystalline colloids known as solution-processed nanoplatelets (NPLs), or colloidal quantum wells, has been introduced.[16] The NPLs have lateral dimensions that are much larger than the exciton Bohr radius of the material (*i.e.*, CdSe, CdTe, CdS, *etc.*) and also than their well-defined and well-controlled vertical thicknesses, typically of several monolayers (MLs).[16,17] Therefore, there exists strong quasi-1D quantum confinement in these NPLs.

Semiconductor NPLs offer advantageous optical properties including narrow photoluminescence emission at room temperature (full-width at half-maximum as small as 30 meV) together with their giant oscillator strength, which are tunable by controlling their vertical thickness.[17−23] Thanks to these favorable features, the NPLs have become appealing for numerous applications including light-emitting diodes[24] and colloidal

lasers.[25−28] To date, core-only NPLs have been extensively studied because of their optimized synthesis conditions available in the literature. Among various investigated properties are electroabsorption,[29] anisotropic optical properties,[30] recombination dynamics,[18] controlled stacking,[31] and excitonic interaction between NPLs.[32] Additionally, various heterostructures have been developed and studied in the form of core/shell and core/crown architectures, allowing for further excitonic engineering.[19,21,33−35] Thus far, vertical-thickness-dependent optical properties have been heavily studied including photoluminescence decay kinetics,[18,20,22,36,37] temperature-dependent trends,[17,18] and exciton−phonon coupling.[23] For example, in the core/crown CdSe/CdS NPLs, optimization of the lateral extent of the crown layer has been shown to be crucial for the stimulated emission.[26] Also, it was reported that increasing the lateral area alters the optical properties of the core/crown CdSe/CdTe NPLs having type II electronic structure.[33,38] In addition, increasing the lateral size in the NPLs has been shown to increase the oscillator strength transition at low temperatures.[39] Furthermore, in the case of the stacked NPLs, the ratio of the phonon emission line intensity to the main emission line increases with increasing lateral size at cryogenic temperature.[40] However, the lateral size dependency of spontaneous emission kinetics and efficiency or stimulated emission performance in CdSe NPLs have not been studied nor elucidated yet. Although the strong quantum confinement in these NPLs is only in the vertical direction, it has thus far remained unknown to what extent the lateral dimensions would affect the optical and excitonic properties in the NPLs and how critical the lateral size is in spontaneous and stimulated emission processes, which are crucial for high performance in light-generating device applications.

Here, we report the systematic lateral size study of optical and excitonic properties of CdSe NPLs in the weak lateral confinement regime for both spontaneous and stimulated emissions. We synthesized CdSe NPLs having different lateral sizes. We observed that the spontaneous emission spectra of the NPLs do not exhibit any significant spectral shift as their lateral size is extended. However, the photoluminescence decay rate was found to strongly accelerate, and PL-QE of these NPLs was observed to considerably decrease with increasing lateral size. These observations strongly suggest the increasing overall nonradiative decay with increasing lateral area. To explain these observations, we have analyzed the PL decay kinetics via considering defected and nondefected NPL subpopulations, revealing that the defected NPL population fraction increases more than 2-fold as the lateral area is increased. With this understanding, we systematically studied both single- and two-photon absorption pumping with increasing lateral size. The NPL ensembles having a smaller defected NPL fraction exhibit a lower amplified
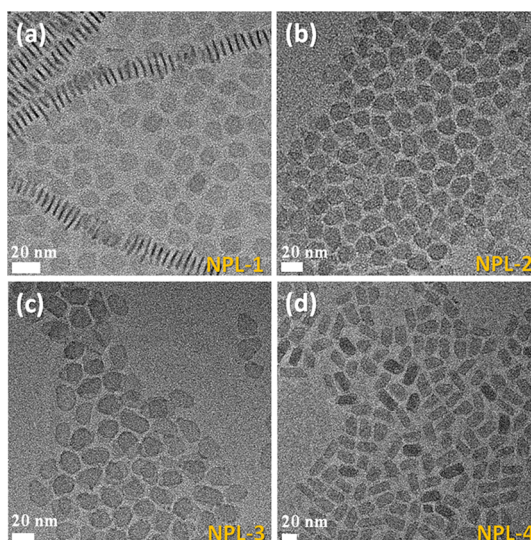

Figure 1. Transmission electron microscopy images of the 4 ML CdSe NPLs having different lateral sizes: (a) 170.0 ± 22.5 nm^2 (NPL-1), (b) 269.6 ± 38.6 nm^2 (NPL-2), (c) 377.6 ± 56.4 nm^2 (NPL-3), and (d) 391.9 ± 65.7 nm^2 (NPL-4), grown using different growth times.

spontaneous emission threshold under single-photon absorption pumping, whereas the NPLs with the larger lateral size achieve a lower threshold for two-photon absorption pumping owing to the giant nonlinear absorption cross-section as high as 2×10^6 GM.

RESULTS AND DISCUSSION

The synthesis of CdSe core-only NPLs having zinc-blende crystal structure was carried out using a modified recipe.[19] CdSe NPLs having different lateral sizes were synthesized using the same recipe with different growth times (see Methods for detail). The vertical thickness and the mean lateral size of the NPLs are extracted from the transmission electron microscopy images (Figure 1). The synthesized CdSe NPLs have the same vertical thickness ($\sim$1.2 nm) corresponding to 4 MLs. This is consistent with the photoluminescence and absorbance peaks in Figure 2.[18,30] The lateral sizes of the NPLs were analyzed to be 170.0 ± 22.5 nm^2 (NPL-1), 269.6 ± 38.6 nm^2 (NPL-2), 377.6 ± 56.4 nm^2 (NPL-3), and 391.9 ± 65.7 nm^2 (NPL-4).

Figure 2 shows the absorbance and steady-state photoluminescence spectra of the NPLs in hexane at room temperature. For each NPL, the absorbance spectrum exhibits two peaks: a sharp peak at 512 nm and the broader peak at 480 nm, corresponding to the electron−heavy hole (e−hh) and the electron−light hole (e−lh) transitions, respectively. The photoluminescence spectra show a single narrow peak at 513 nm, resulting from the radiative recombination at the electron−heavy hole transition,[17] with a very small Stokes shift ($\sim$1 nm). As the lateral size of the NPLs grows larger, the photoluminescence emission peak does not change its spectral position. Also, the full-width-at-half-maxima
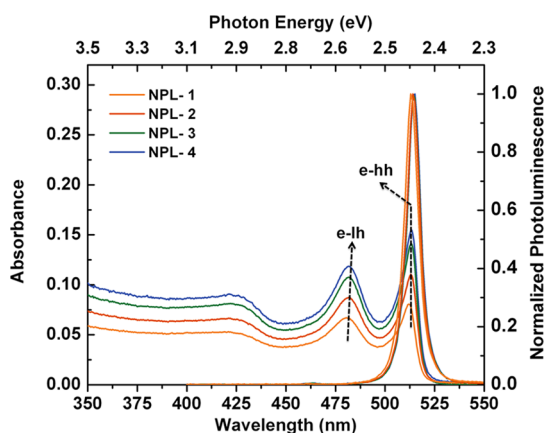
Figure 2. Absorption and photoluminescence spectra of the 4 ML CdSe NPLs grown in the lateral direction with different growth times. The peaks labeled as e−lh and e−hh in the absorption spectrum correspond to the electron−light hole and the electron−heavy hole transitions, respectively.

(fwhm) of the photoluminescence emission peaks remains unchanged (∼8 nm). Detailed information for the absorption and photoluminescence spectra is given in the Supporting Information (see Table S1). Having the same features in the UV−vis and the photoluminescence spectra with growing lateral size suggests weak quantum confinement in the lateral plane owing to the fact that the lateral dimensions are much larger than the exciton Bohr radius of CdSe.[39,41]

To understand the fluorescence decay kinetics of the NPLs as a function of the changing lateral size, time-resolved fluorescence spectroscopy using the time-correlated single photon counting system was performed (Figure 3). Here we used a pulsed pump laser (375 nm, 2.5 MHz repetition rate, <100 ps pulse width) to excite the diluted NPL solutions in hexane. The exciton density per NPL is very small ($\langle N \rangle \ll 1$) due to the very low intensity of the pump laser. Figure 3a shows the fluorescence decay curves measured at the peak emission wavelength (∼513 nm) of the NPLs for four different samples. The fluorescence decay curves of the NPLs were numerically fitted with multiexponential decay functions, indicating the presence of multiple decay channels in the ensemble of the NPLs. The fitting parameters are given in Table S2. The multiexponential decay behavior in both a single NPL and an ensemble of NPLs was previously reported.[23,37,41] Tessier et al. have performed single-NPL-based time-resolved fluorescence spectroscopy and measured PL decay curves that could be fitted by three-exponential decay functions.[41] This indicates that individual NPLs exhibit complex decay dynamics possibly due to the presence of more than one radiative channel (i.e., direct radiative recombination and trap-related radiative recombination) in addition to nonradiative (i.e., electron and hole traps) channels present in the NPL ensembles. Figure 3b presents the fluorescence lifetime components of the measurement in different NPL ensembles

of varying mean lateral size. These four exponential decay components have distinct lifetimes: ∼90, ∼16, ∼4, and ∼0.5 ns. The amplitude-averaged photoluminescence lifetime (τ_{av}) of the NPL ensembles with increasing lateral size is presented in Figure 3c, showing that the τ_{av} decreases from 7.61 ns to 2.73 ns as the mean lateral size of the NPLs is increased. This shortening in the photoluminescence lifetime was previously reported in epitaxial quantum wells that was studied as a function of well thickness.[42] In the colloidal NPLs, photoluminescence lifetime has been studied as a function of temperature, revealing the giant oscillator strength transition in these materials, although lateral size dependence has not been understood to date.[17,39,41]

One possible hypothesis to explain the accelerated photoluminescence decay rates with extended lateral size is the increasing radiative rates due to increasing oscillator strength. To check this hypothesis, photoluminescence quantum efficiency of different NPL ensembles was measured using a reference dye, rhodamine 6G (Rh6G), having 95% PL-QE in its very diluted ethanol solution at room temperature (see Figure S1). Previously in core-only NPLs, PL-QE was reported to be 30−50%.[16,17,27,40,43] However, the relation between the PL-QE and the lateral size of the NPLs has not been studied. Here, we find that the PL-QE substantially decreases from 76.8% to 33.3% as the lateral size of the NPLs increases (see Figure 3d). This shows that the hypothesis concerning increasing radiative rates cannot be correct. Thus, the observed strong decrease of the PL-QE in the larger lateral size NPLs cannot be accounted for by the increasing oscillator strength. The decrease in the PL-QE of the NPLs together with the accelerated photoluminescence decay rates strongly suggests the increased overall nonradiative recombination in these NPLs. A simple calculation (PL-QE = $\gamma_{Rad}/(\gamma_{Rad} + \gamma_{Nonrad})$) indicates that the effective nonradiative decay rate increases by 8-fold in the larger lateral area NPLs (i.e., NPL-4) as compared to the smaller ones (i.e., NPL-1), whereas the radiative decay rate (and, thus, the oscillator strength) increases by only 1.2-fold.

To understand the effect of nonradiative recombination channels in the NPLs, we look into the exponential photoluminescence decay components and their steady-state contributions, which are quantified with $A_i \times \tau_i$ products (i = 1 to 4), where A_i represents the amplitude of the exponential decay and τ_i is its characteristic lifetime, extracted from numerical fits to the photoluminescence decay curves using the relation

$$PL(t) = \sum_i A_i e^{-t/\tau_i}$$
$$A_i \times \tau_i = \int A_i e^{-t/\tau_i}$$

(1)

Each $A_i \times \tau_i$ term corresponds to the area under the corresponding exponential decay curve, giving its specific steady-state contribution within the total
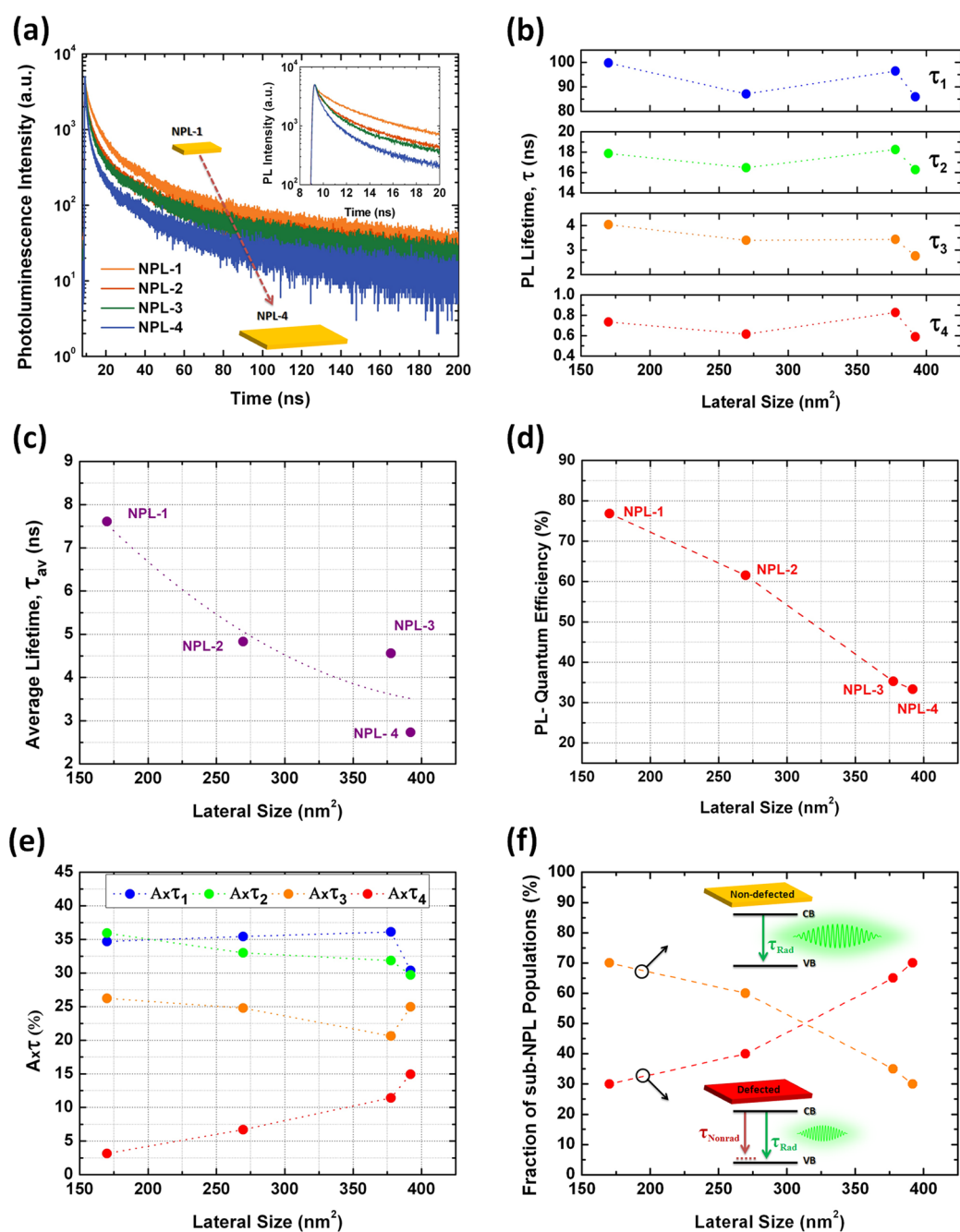
Figure 3. (a) Time-resolved fluorescence (TRF) decays of the NPLs having different lateral sizes. The inset shows the zoom-in of the same TRF decay. Evolution of (b) the lifetime components of fluorescence decays, (c) the amplitude-averaged photoluminescence lifetimes, (d) photoluminescence quantum efficiency (PL-QE), (e) the percentage steady-state contribution from each decay component of the NPLs, and (f) calculated fraction of NPL subpopulations as a function of the lateral size. The dotted lines are a guide for the eyes.

emission. Figure 3e exhibits the fractional change of the steady-state contribution of each lifetime component for four different NPL samples being studied here. As the size of the NPLs is increased, the relative contribution of the $A_4 \times \tau_4$ term increases from 3.15% to 14.94%. The fractional contributions of other lifetime components (i.e., $A_1 \times \tau_1$, $A_2 \times \tau_2$, and $A_3 \times \tau_3$) are observed to decrease with increasing lateral size. An increasing contribution from the $A_4 \times \tau_4$ term as the PL-QE decreases would strongly imply that the τ_4

component, which is the fastest lifetime, is related to a nonradiative decay channel within the NPL population. For example, fast hole trapping is widely observed in Cd-based NCs especially due to poor surface passivation and Cd vacancies.[44−46] Recently, Kunneman et al. have also shown that a large fraction of the NPL populations contains NPLs with hole traps exhibiting lifetimes on the order of 10's or 100's of picoseconds.[36] As the lateral size of an NPL is increased, the probability of finding a hole trap state such as a Cd vacancy within

that NPL would be increasing. Therefore, the population fraction of the NPLs having hole traps would be higher in an NPL ensemble having a larger mean lateral size, which would in turn strongly decrease the ensemble PL-QE. Recently, we have shown that such defected NPLs can strongly quench the photoluminescence emission of the stacked NPLs due to ultrafast exciton transport within the stacked NPLs through Förster resonance energy transfer.[31] The lateral-size-dependent photoluminescence decay components (τ_i) and fractional emission contributions (($A_i \times \tau_i$)/($\Sigma A_i \times \tau_i$)), which are listed in Table S2, indicate that while the lifetime components do not change significantly as a function of the lateral size (see Figure 3b), the fractional emission contributions do (see Figure 3e). Therefore, the amplitude average lifetimes change considerably with the lateral size. The shortening in the amplitude average lifetimes might be explained by changing relative contributions of the lifetime components due to the changing population fractions of the defected and nondefected NPLs in the ensemble. With increasing lateral size, the number of defected NPLs grows larger. As a result, the overall nonradiative channels in the NPL ensembles are increased with the increased lateral size. We also observe exactly the same lateral-size-dependent behavior in the NPL populations synthesized using the core-seeded approach (see Tables S3 and S4 and Figure S2 and related discussion in the Supporting Information). Similarly, such complex PL decay kinetics have been previously observed in the CdSe NCs[47,48] and in CdSe NPLs[31,36] arising due to dynamic surface trapping. Furthermore, the surface trapping in the NCs has been shown to be highly sensitive to temperature and time since these can excitonically alter the heterogeneity of the NC populations.

To develop a better insight, we quantitatively calculate the change of the NPL subpopulations for the different NPL ensembles. Here, we assume that the NPL population consists of two types of NPLs: nondefected and defected (*i.e.*, having rapid nonradiative recombination).[31,36] Previously, the Dubertret group has observed the presence of three distinct fluorescence lifetime components in emissive NPLs *via* single-particle measurements.[41] These lifetime components match very well with τ_1 (80–100 ns), τ_2 (15–18 ns), and τ_3 (1–3 ns) lifetime components that we found in our work. Therefore, we relate these lifetime components (τ_1, τ_2, and τ_3) as the distinct radiative states in nondefected NPLs. In the case of defected NPLs, the fastest lifetime component, τ_4 (0.6–0.8 ns), is attributed to the nonradiative channel (*i.e.*, hole trapping) since its contribution significantly increases (from 3% to 15%) as the PL-QE of the NPLs decreases. We assume that x% of the NPL population consists of nondefected NPLs. and the rest, $(1 - x)$%, consists of defected NPLs (see Figure S3). Nondefected NPLs are assumed to have a PL-QE of 100% and exhibit only τ_1, τ_2, and τ_3 lifetime components. On the other hand, defected NPLs have the fast nonradiative lifetime of τ_4 in addition to three distinct radiative lifetime components. The PL-QE in the defected NPLs is found by considering that the nonradiative channel (τ_4) would compete with each of the radiative channels (τ_1, τ_2, and τ_3) individually. Therefore, τ_1–τ_4, τ_2–τ_4, and τ_3–τ_4 combinations (see Figure S3) would result in PL-QEs (PL-QE = $\gamma_{Rad}/(\gamma_{Rad} + \gamma_{Nonrad})$) of ~0.7%, ~3.5%, and ~18%, respectively. Considering that these three distinct radiative emission channels have almost equal contribution to the total radiative emission, which can be justified by considering their almost equal fractional emission contributions as shown in Table S2, the PL-QE of a defected NPL would be calculated to be ~8%. We match the calculated PL-QEs to experimentally measured PL-QEs for the different NPL samples (NPL-1, -2, -3, and -4) *via* choosing the population fraction (x%) of the nondefected and $((1 - x)$%) defected NPLs properly (PL-QE = 100% $\times x +$ 8% $\times (1 - x)$). We observe that NPL-1 has the lowest defected NPL population fraction (~30%) since it has the highest PL-QE. As the lateral area of the NPL samples increases, the defected NPL population fraction increases up to 70% (for the NPL-4) (see Figure 3f). This explains the significantly reduced PL-QEs in the larger lateral area NPLs. Furthermore, to check the consistency of the calculated defected and nondefected NPL subpopulation fractions with the time-resolved fluorescence measurements, we calculated the contribution of the fluorescence lifetime components to the total emission of the NPL ensemble (see Table S5) for the two NPL subpopulations. In this calculation, we assumed the contributions of the radiative channels τ_1, τ_2, and τ_3 to the total emission to be almost equal (*i.e.*, 35%, 35%, and 30%, respectively). We justify this by the observation of the fractional contributions of the τ_1, τ_2, and τ_3 lifetime components from the experimental data in Table S2. In the case of the contribution of the lifetime components to the total emission in the defected NPLs, the presence of the fast nonradiative τ_4 component and the low PL-QE (~8%) are considered. In Table S6, we summarize the calculated emission contributions of all lifetime components for the four different NPL ensembles, and the calculated values were compared to the experimental ones. The calculated emission contributions exhibit a very good match with the experimental ones. Therefore, the change of the population fraction of the defected NPLs causes the reduced PL-QEs in the increased lateral area NPLs. This good agreement between the calculated and the experiment data for each NPL ensemble (NPL-1, -2, -3, and -4) exhibits strong support for the hypothesis that the nonradiative decay pathways dictate the decreasing trend in the PL-QE due to poorly passivated surfaces (acting as fast hole traps) becoming dominantly stronger with increasing lateral size.

Recently, optical gain has been shown in the colloidal NPLs independently by She *et al.*[25] using core/shell

architecture and Guzelturk et al.[26] using core/crown architecture. A record high optical gain coefficient among all colloidal optical gain media, which is as high as 650 cm^{-1}, has been achieved using the core/crown NPLs.[26] Most recently, Grim et al. have shown that continuous wave pumped optical gain is possible in the NPL-based gain media.[27] These recent works strongly suggest that colloidal NPLs are extremely promising materials for lasers.[26,27] However, the dependency of the optical gain threshold, at which pump intensity of the amplified spontaneous emission (ASE) can be initiated, on the lateral area of the NPLs has not previously been elucidated. Here, we studied the optical gain performance of the CdSe NPLs having varying lateral sizes. To this end, we investigated both single- and two-photon absorption pumped ASE (1PA- and 2PA-ASE) in the NPL samples mentioned above. We prepared solid film samples of the NPLs (i.e., NPL-1, NPL-2, NPL-3, and NPL-4) on glass substrates via drop-casting from concentrated solutions.

Single-photon absorption pumped (400 nm, 120 fs, 1 kHz) ASE measurements were performed via using a stripe excitation configuration to excite the samples through a cylindrical lens (f = 20 cm). We used a variable neutral density filter before the cylindrical lens to adjust the excitation intensity. The pump-intensity-dependent emission spectra are presented in Figure 4a for the exemplary case of NPL-1. In 4 ML thick CdSe NPLs, the ASE peak was observed at ~532 nm arising due to the biexcitonic optical gain.[26,27] Here, in accordance with the previous reports, we observed a red-shifted ASE peak that has a fwhm as narrow as 6 nm at room temperature. The transition from the spontaneous emission to the stimulated emission is visible for the excitation intensities higher than 45 μJ/cm^2. The emission intensity vs single-photon pump intensity measurements are shown in Figure 4b for all of the NPLs. The 1PA-ASE threshold is the lowest for the NPL-1, which has the smallest lateral size. As the lateral size is increased, the ASE threshold becomes progressively larger (see Figure 4c). This indicates that for single-photon absorption pumping there is a strong correlation between the PL-QEs of the NPLs and the stimulated emission thresholds. As the NPL lateral size is increased, the defected NPL (i.e., NPL with a fast nonradiative trap channel) population also increases in number. Therefore, in the dense solid-state films of the NPLs, which are required for optical gain purposes, strong nonradiative energy transfer among the same type of NPLs can quench the emission considerably.[31] Thus, NPL populations having a lower defected NPL fraction will be favorable for optical gain and light-generation application.

We also performed two-photon absorption pumping (800 nm, 120 fs, 1 kHz) to realize frequency up-converted ASE in the NPLs, which is interesting for nonlinear optical applications including frequency up-converted

lasers and bioimaging. Recently, 2PA-ASE has been shown to be possible in the NPLs by our group.[26] However, the lateral size dependency of the frequency up-converted optical gain has not been considered before. In the nonlinear processes, such as two-photon absorption, the physical volume becomes critical.[28,49−51] Therefore, one might expect to observe different trends for the two-photon-pumped optical gain performance of the NPLs as compared to single-photon pumping. Figure 4d shows the emission spectra of the exemplary case of NPL-4 for different pump intensities, revealing the transition from spontaneous to stimulated emission. The emission intensity vs two-photon pump intensity measurements are depicted for all four NPLs in Figure 4e. The 2PA-ASE threshold is found to be the lowest for NPL-4, which has the largest lateral size. As the lateral size is decreased, the threshold for ASE increases (see Figure 4f). This shows an opposite trend of that of 1PA-ASE. Increasing the lateral size of the NPLs is important for boosting the nonlinear optical response. Therefore, larger area NPLs offer better response in terms of optical gain threshold despite the increasing overall nonradiative decay channels in the ensemble. The single- and two-photon absorption pumped ASE thresholds are given in Table S7.

To understand the trend of decreasing 2PA-ASE threshold with increasing lateral size, we measured the two photon absorption (2PA) cross-section of the NPL ensembles by open-aperture z-scan technique (see the SI for the details of the experiment). We dissolved 0.497 μM (NPL-2) and 0.299 μM (NPL-4) solutions of the NPL ensembles in hexane in a 1 mm quartz cuvette. The concentrations of the NPL solutions were determined via analysis of the concentration by the elemental analysis using inductively coupled plasma optical emission spectroscopy. We fit the normalized transmittance data using eq S1. The two-photon absorption cross-section of the smaller NPL ensemble (NPL-2) is found to be 0.537 × 10^6 GM (1 GM = 10^{-58} m^4 × s × photon^{-1}), while 2.247 × 10^6 GM is measured for the largest NPL ensemble (NPL-4). This comparative measurement shows that the 2PA cross-section grows overwhelmingly stronger with increasing lateral size and reaches extraordinarily high levels. To the best of our knowledge, this "giant" two-photon absorption cross-section measured in our largest NPL ensemble is the highest reported nonlinear absorption cross-section in all colloidal semiconductor NCs. Previously, in the case of colloidal quantum dots, a two-photon absorption cross-section was measured to be up to 50 000 GM.[28] In the case of colloidal nanorods, the two-photon absorption cross-section was found to be as high as 2.3 × 10^5 GM.[52] In the organic semiconductors, the maximum two-photon absorption cross-section was reported up to 10^6 GM.[53] Therefore, this giant two-photon absorption cross-section makes colloidal NPLs highly attractive and suitable materials for
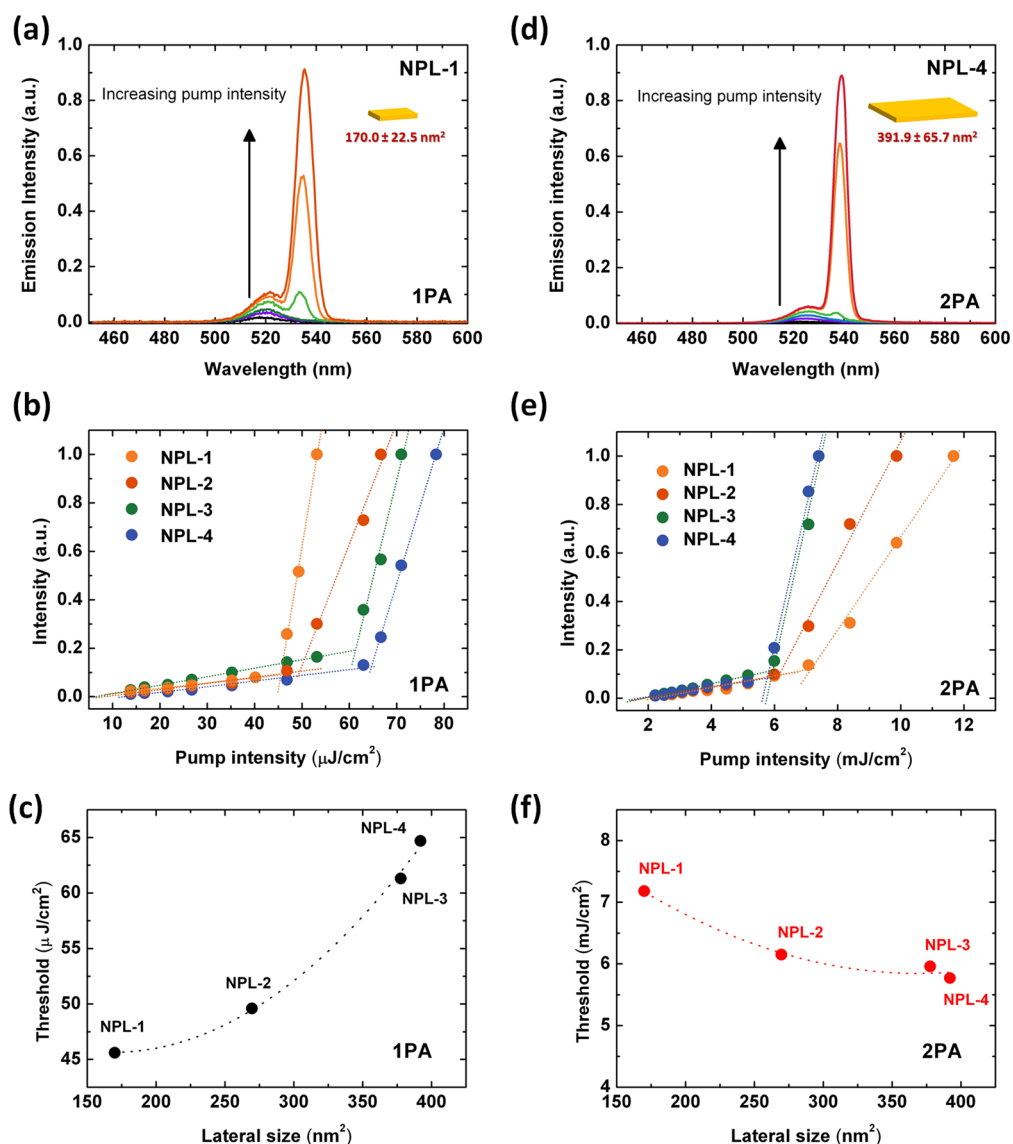
Figure 4. (a) Single-photon absorption (1PA) pumped ASE of the 4 ML CdSe NPLs (NPL-1) having a lateral size of 170.0 nm². (b) 1PA-pumped luminescence *vs* pump intensity of the NPLs having different lateral size. (c) Evolution of the 1PA-pumped ASE thresholds with lateral size. (d) Two-photon absorption (2PA) pumped ASE of the NPL-4 having a lateral size of 391.9 nm². (e) 2PA-pumped luminescence *vs* pump intensity of the NPLs having different lateral size. (f) Evolution of the 2PA-pumped ASE thresholds with lateral size. The dotted lines are a guide for the eyes. The 1PA- and 2PA-ASE thresholds exhibit opposite trends for varying lateral size.

bioimaging in deep tissues *via* using near-infrared (NIR) sources. To understand the observed unprecedented nonlinear optical properties further, our detailed studies are currently ongoing.

CONCLUSION

In summary, we have investigated the effect of lateral size variation on the optical and excitonic properties of the colloidal CdSe NPLs having 4 ML of thickness for both spontaneous and stimulated emissions. In the spontaneous emission, we found an accelerating photoluminescence decay rate and decreasing PL-QE at room temperature with increasing lateral size. Contrary to expectations, this reveals that the nonradiative channels dictate the observed trend
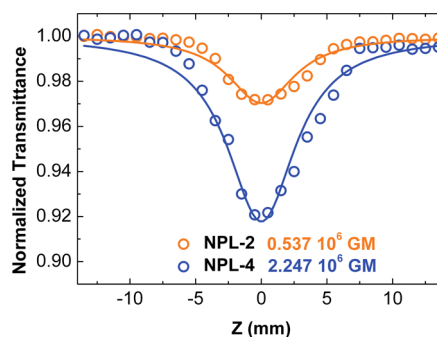

Figure 5. Comparative open-aperture *z*-scan measurement of the NPL ensembles having lateral areas of 269.6 nm² (NPL-2) and 391.9 nm² (NPL-4). The fit of the *z*-scan measurement gives a giant two-photon absorption cross-section of 0.537 × 10⁶ GM and 2.247 × 10⁶ GM for the NPL-2 and NPL-4, respectively.

due to increasing fraction of the defected NPL sub-population with extended lateral size. In the case of stimulated emission, both the single- (1PA) and two-photon absorption (2PA) pumping ASE measurements exhibit size-dependent behavior. However, their ASE threshold trends over varying laterals size are completely opposite. The NPLs with a larger lateral size show a higher threshold in 1PA-pumped ASE due to their decreased quantum efficiency, as compared to the smaller ones. On the other hand, the larger NPLs enable a lower threshold in 2PA-pumped ASE owing to their strongly increased nonlinear absorption cross-section. This increase is so large that the nonlinear absorption cross-section reaches record high levels above 10^6 GM.

Lateral size control of the NPLs, therefore, proves to be critical in the resulting optical and excitonic properties. The vertical dimension of the NPLs, though leading to the strong quantum confinement, does not alone set the properties of spontaneous and stimulated emissions. In particular, a careful selection of the NPL lateral size is essential to low-threshold 1PA- and 2PA-ASE. Also, the "giant" nonlinear absorption cross-section observed in the NPLs, measured here as high as 2.25×10^6 GM for a lateral size of $\sim$392 nm^2, is at least an order of magnitude stronger than those of colloidal quantum dots and rods reported to date. We believe that these new findings will help to realize high-performance solution-processed NPL devices.

METHODS

Synthesis of the 4 ML CdSe NPLs. For a typical synthesis, 170 mg of cadmium myristate, 12 mg of selenium, and 15 mL of octadecene (ODE) are loaded into a three-neck flask. After evacuation of the mixed solution at room temperature for 1 h, it is heated to 240 °C under argon atmosphere. When the temperature reaches 195 °C, the color of the solution becomes yellowish, and 55 mg of cadmium acetate dihydrate is introduced swiftly into the reaction. After 2, 4, 6, and 8 min of growth of CdSe NPLs for NPL-1, NPL-2, NPL-3, and NPL-4 at 240 °C, respectively, the reaction is stopped and cooled to room temperature with the injection of 0.5 mL of oleic acid (OA). The resulting 4 ML CdSe NPLs are separated by other reaction products with successive purification steps. First, the resulting mixture is centrifuged at 14 500 rpm for 10 min, and the supernatant is removed from the centrifuge tube. The precipitate is dried under nitrogen, dissolved in hexane, and centrifuged again at 4500 rpm for 5 min. In the second step, the supernatant is separated into another centrifuge tube, and ethanol is added into the supernatant solution until it becomes turbid. In the last step, after the turbid solution is centrifuged at 4500 rpm for 5 min, the precipitate is dissolved in hexane and filtered with a 0.20 μm filter.

Core-Seeded Approach for Growth of the 4 ML CdSe NPLs in Lateral Dimensions. The synthesis of the 4 ML CdSe having different lateral sizes with the crown-like growth process is performed with the injection of cadmium and selenium precursors, which are prepared with a modified recipe.[19] The starting core-only 4 ML CdSe NPLs (csNPL-1) are synthesized using 40 mg of cadmium acetate dihydrate for 5 min growing time. A certain amount of NPLs that is dissolved in hexane and 5 mL of ODE is loaded into a three-neck flask. The solution is degassed to remove all hexane, water, and oxygen inside the solution. Then, under an argon atmosphere, the solution is heated to 240 °C. When the temperature reaches 240 °C, 0.25 mL (for csNPL-2) and 0.50 mL (for csNPL-3) of Cd—Se precursors are injected at a rate of 4 mL/h. After the injection of Cd—Se precursors, the reaction is stopped with the injection of 0.5 mL of OA and the system is cooled to room temperature. The resulting NPLs are purified with successive purification steps as described before.

Conflict of Interest: The authors declare no competing financial interest.

Supporting Information Available: Detailed information about the absorption and photoluminescence spectra and numerical analysis of time-resolved fluorescence of all samples used in this study, details of the PL-QE measurements, calculation of NPL subpopulation fractions and their lifetime contributions, both single- and two-photon absorption pumped ASE threshold values of the NPLs having different lateral sizes, and details of the open-aperture *z*-scan measurements. The Supporting Information is available free of charge on the ACS Publications website at DOI: 10.1021/acsnano.5b01927.

REFERENCES AND NOTES

1. Murray, C. B.; Norris, D. J.; Bawendi, M. G. Synthesis and Characterization of Nearly Monodisperse CdE (E = S, Se, Te) Semiconductor Nanocrystallites. *J. Am. Chem. Soc.* **1993**, *115*, 8706–8715.
2. Colvin, V. L.; Schlamp, M. C.; Alivisatos, A. P. Light-Emitting Diodes Made from Cadmium Selenide Nanocrystals and a Semiconducting Polymer. *Nature* **1994**, *370*, 354–357.
3. Klimov, V. I.; Mikhailosvsky, A. A.; Xu, S.; Malko, A.; Hollingsworth, J. A.; Leatherdale, C. A.; Eisler, H. J.; Bawendi, M. G. Optical Gain and Stimulated Emission in Nanocrystal Quantum Dots. *Science* **2000**, *290*, 314–317.
4. Semonin, O. E.; Luther, J. M.; Choi, S.; Chen, H.-Y.; Gao, J.; Nozik, A. J.; Beard, M. C. Peak External Photocurrent Quantum Efficiency Exceeding 100% *via* MEG in a Quantum Dot Solar Cell. *Science* **2011**, *334*, 1530–1533.
5. Dai, X.; Zhang, Z.; Jin, Y.; Niu, Y.; Cao, H.; Liang, X.; Chen, L.; Wang, J.; Peng, X. Solution-Processed, High-Performance Light-Emitting Diodes Based on Quantum Dots. *Nature* **2014**, *515*, 96–99.
6. Lim, J.; Jeong, B. G.; Park, M.; Kim, J. K.; Pietryga, J. M.; Park, Y.-S.; Klimov, V. I.; Lee, C.; Lee, D. C.; Bae, W. K. Influence of Shell Thickness on the Performance of Light-Emitting Devices Based on CdSe/Zn1-X CdX S Core/Shell Heterostructured Quantum Dots. *Adv. Mater.* **2014**, *26*, 8034–8040.
7. Norris, D.; Bawendi, M. Measurement and Assignment of the Size-Dependent Optical Spectrum in CdSe Quantum Dots. *Phys. Rev. B* **1996**, *53*, 16338–16346.
8. Yu, W. W.; Qu, L.; Guo, W.; Peng, X. Experimental Determination of the Extinction Coefficient of CdTe, CdSe, and CdS Nanocrystals. *Chem. Mater.* **2003**, *15*, 2854–2860.
9. Robel, I.; Gresback, R.; Kortshagen, U.; Schaller, R. D.; Klimov, V. I. Universal Size-Dependent Trend in Auger Recombination in Direct-Gap and Indirect-Gap Semiconductor Nanocrystals. *Phys. Rev. Lett.* **2009**, *102*, 177404.
10. Jasieniak, J.; Smith, L.; van Embden, J.; Mulvaney, P.; Califano, M. Re-examination of the Size-Dependent Absorption Properties of CdSe Quantum Dots. *J. Phys. Chem. C* **2009**, *113*, 19468–19474.
11. Leistikow, M.; Johansen, J.; Kettelarij, A.; Lodahl, P.; Vos, W. Size-Dependent Oscillator Strength and Quantum

Efficiency of CdSe Quantum Dots Controlled *via* the Local Density of States. *Phys. Rev. B* **2009**, *79*, 045301.

12. Gong, K.; Zeng, Y.; Kelley, D. F. Extinction Coefficients, Oscillator Strengths, and Radiative Lifetimes of CdSe, CdTe, and CdTe/CdSe Nanocrystals. *J. Phys. Chem. C* **2013**, *117*, 20268–20279.

13. Kambhampati, P. Hot Exciton Relaxation Dynamics in Semiconductor Quantum Dots: Radiationless Transitions on the Nanoscale. *J. Phys. Chem. C* **2011**, *115*, 22089–22109.

14. Kambhampati, P. Multiexcitons in Semiconductor Nanocrystals: A Platform for Optoelectronics at High Carrier Concentration. *J. Phys. Chem. Lett.* **2012**, *3*, 1182–1190.

15. Kambhampati, P. Unraveling the Structure and Dynamics of Excitons in Semiconductor Quantum Dots. *Acc. Chem. Res.* **2011**, *44*, 1–13.

16. Ithurria, S.; Dubertret, B. Quasi 2D Colloidal CdSe Platelets with Thicknesses Controlled at the Atomic Level. *J. Am. Chem. Soc.* **2008**, *130*, 16504–16505.

17. Ithurria, S.; Tessier, M. D.; Mahler, B.; Lobo, R. P. S. M.; Dubertret, B.; Efros, A. L. Colloidal Nanoplatelets with Two-Dimensional Electronic Structure. *Nat. Mater.* **2011**, *10*, 936–941.

18. Biadala, L.; Liu, F.; Tessier, M. D.; Yakovlev, D. R.; Dubertret, B.; Bayer, M. Recombination Dynamics of Band Edge Excitons in Quasi-Two-Dimensional CdSe Nanoplatelets. *Nano Lett.* **2014**, *14*, 1134–1139.

19. Tessier, M. D.; Spinicelli, P.; Dupont, D.; Patriarche, G.; Ithurria, S.; Dubertret, B. Efficient Exciton Concentrators Built from Colloidal Core/Crown CdSe/CdS Semiconductor Nanoplatelets. *Nano Lett.* **2014**, *14*, 207–213.

20. Kunneman, L. T.; Tessier, M. D.; Heuclin, H.; Dubertret, B.; Aulin, Y. V.; Grozema, F. C.; Schins, J. M.; Siebbeles, L. D. A. Bimolecular Auger Recombination of Electron−Hole Pairs in Two-Dimensional CdSe and CdSe/CdZnS Core/Shell Nanoplatelets. *J. Phys. Chem. Lett.* **2013**, *4*, 3574–3578.

21. Mahler, B.; Nadal, B.; Bouet, C.; Patriarche, G.; Dubertret, B. Core/Shell Colloidal Semiconductor Nanoplatelets. *J. Am. Chem. Soc.* **2012**, *134*, 18591–18598.

22. Pelton, M.; Ithurria, S.; Schaller, R. D.; Dolzhnikov, D. S.; Talapin, D. V. Carrier Cooling in Colloidal Quantum Wells. *Nano Lett.* **2012**, *12*, 6158–6163.

23. Achtstein, A. W.; Schliwa, A.; Prudnikau, A.; Hardzei, M.; Artemyev, M. V.; Thomsen, C.; Woggon, U. Electronic Structure and Exciton-Phonon Interaction in Two-Dimensional Colloidal CdSe Nanosheets. *Nano Lett.* **2012**, *12*, 3151–3157.

24. Chen, Z.; Nadal, B.; Mahler, B.; Aubin, H.; Dubertret, B. Quasi-2D Colloidal Semiconductor Nanoplatelets for Narrow Electroluminescence. *Adv. Funct. Mater.* **2014**, *24*, 295–302.

25. She, C.; Fedin, I.; Dolzhnikov, D. S.; Demortière, A.; Schaller, R. D.; Pelton, M.; Talapin, D. V. Low-Threshold Stimulated Emission Using Colloidal Quantum Wells. *Nano Lett.* **2014**, *14*, 2772–2777.

26. Guzelturk, B.; Kelestemur, Y.; Olutas, M.; Delikanli, S.; Demir, H. V. Amplified Spontaneous Emission and Lasing in Colloidal Nanoplatelets. *ACS Nano* **2014**, *8*, 6599–6605.

27. Grim, J. Q.; Christodoulou, S.; Di Stasio, F.; Krahne, R.; Cingolani, R.; Manna, L.; Moreels, I. Continuous-Wave Biexciton Lasing at Room Temperature Using Solution-Processed Quantum Wells. *Nat. Nanotechnol.* **2014**, *9*, 891–895.

28. Guzelturk, B.; Kelestemur, Y.; Gungor, K.; Yeltik, A.; Akgul, M. Z.; Wang, Y.; Chen, R.; Dang, C.; Sun, H.; Demir, H. V. Stable and Low-Threshold Optical Gain in CdSe/CdS Quantum Dots: An All-Colloidal Frequency Up-Converted Laser. *Adv. Mater.* **2015**, *27*, 2741–2746.

29. Achtstein, A. W.; Prudnikau, A. V.; Ermolenko, M. V.; Gurinovich, L. I.; Gaponenko, S. V.; Woggon, U.; Baranov, A. V.; Leonov, M. Y.; Rukhlenko, I. D.; Federov, A. V.; *et al.* Electroabsorption by 0D, 1D, and 2D Nanocrystals: A Comparative Study of CdSe Colloidal Quantum Dots, Nanorods and Nanoplatelets. *ACS Nano* **2014**, *8*, 7678–7686.

30. Abecassis, B.; Tessier, M. D.; Davidson, P.; Dubertret, B. Self-Assembly of CdSe Nanoplatelets into Giant Micrometer-Scale Needles Emitting Polarized Light. *Nano Lett.* **2014**, *14*, 710–715.

31. Guzelturk, B.; Erden, O.; Olutaş, M.; Kelestemur, Y.; Demir, H. V. Stacking in Colloidal Nanoplatelets: Tuning Excitonic Properties. *ACS Nano* **2014**, *8*, 12524–12533.

32. Guzelturk, B.; Olutas, M.; Delikanli, S.; Kelestemur, Y.; Erden, O.; Demir, H. V. Nonradiative Energy Transfer in Colloidal CdSe Nanoplatelet Films. *Nanoscale* **2015**, *7*, 2545–2551.

33. Pedetti, S.; Ithurria, S.; Heuclin, H.; Patriarche, G.; Dubertret, B. Type-II CdSe/CdTe Core/Crown Semiconductor Nanoplatelets. *J. Am. Chem. Soc.* **2014**, *136*, 16430–16438.

34. Prudnikau, A.; Chuvilin, A.; Artemyev, M. CdSe−CdS Nano-heteroplatelets with Efficient Photoexcitation of Central CdSe Region through Epitaxially Grown CdS Wings. *J. Am. Chem. Soc.* **2013**, *135*, 14476–14479.

35. Ithurria, S.; Talapin, D. V. Colloidal Atomic Layer Deposition (c-ALD) Using Self-Limiting Reactions at Nanocrystal Surface Coupled to Phase Transfer between Polar and Nonpolar Media. *J. Am. Chem. Soc.* **2012**, *134*, 18585–18590.

36. Kunneman, L. T.; Schins, J. M.; Pedetti, S.; Heuclin, H.; Grozema, F. C.; Houtepen, A. J.; Dubertret, B.; Siebbeles, L. D. A. Nature and Decay Pathways of Photoexcited States in CdSe and CdSe/CdS Nanoplatelets. *Nano Lett.* **2014**, *14*, 7039–7045.

37. Tessier, M. D.; Mahler, B.; Nadal, B.; Heuclin, H.; Pedetti, S.; Dubertret, B. Spectroscopy of Colloidal Semiconductor Core/Shell Nanoplatelets with High Quantum Yield. *Nano Lett.* **2013**, *13*, 3321–3328.

38. Kelestemur, Y.; Olutas, M.; Delikanli, S.; Guzelturk, B.; Akgul, M. Z.; Demir, H. V. Type-II Colloidal Quantum Wells: CdSe/CdTe Core/Crown Heteronanoplatelets. *J. Phys. Chem. C* **2015**, *119*, 2177–2185.

39. Naeem, A.; Masia, F.; Christodoulou, S.; Moreels, I.; Borri, P.; Langbein, W. Giant Exciton Oscillator Strength and Radiatively Limited Dephasing in Two-Dimensional Platelets. *Phys. Rev. B* **2015**, *91*, 121302(R).

40. Tessier, M. D.; Biadala, L.; Bouet, C.; Ithurria, S.; Abecassis, B.; Dubertret, B. Phonon Line Emission Revealed by Self-Assembly of Colloidal Nanoplatelets. *ACS Nano* **2013**, 3332–3340.

41. Tessier, M. D.; Javaux, C.; Maksimovic, I.; Loriette, V.; Dubertret, B. Spectroscopy of Single CdSe Nanoplatelets. *ACS Nano* **2012**, *6*, 6751–6758.

42. Feldmann, J.; Peter, G.; Gobel, E. O. Linewidth Dependence of Radiative Exciton Lifetimes in Quantum Wells. *Phys. Rev. Lett.* **1987**, *59*, 2337–2340.

43. Ithurria, S.; Bousquet, G.; Dubertret, B. Continuous Transition from 3D to 1D Confinement Observed during the Formation of CdSe Nanoplatelets. *J. Am. Chem. Soc.* **2011**, *133*, 3070–3077.

44. Hines, D. A.; Kamat, P. V. Quantum Dot Surface Chemistry: Ligand Effects and Electron Transfer Reactions. *J. Phys. Chem. C* **2013**, *117*, 14418–14426.

45. Knowles, K. E.; Mcarthur, E. A.; Weiss, E. A. A Multi-Timescale Map of Radiative and Nonradiative Decay Pathways for Excitons in CdSe Quantum Dots. *ACS Nano* **2011**, *5*, 2026–2035.

46. Vietmeyer, F.; Tchelidze, T.; Tsou, V.; Janko, B.; Kuno, M. Electric Field-Induced Emission Enhancement and Modulation in Individual CdSe Nanowires. *ACS Nano* **2012**, *6*, 9133–9140.

47. Kambhampati, P. On the Kinetics and Thermodynamics of Excitons at the Surface of Semiconductor Nanocrystals: Are There Surface Excitons? *Chem. Phys.* **2015**, *446*, 92–107.

48. Mooney, J.; Krause, M. M.; Kambhampati, P. Connecting the Dots: The Kinetics and Thermodynamics of Hot, Cold, and Surface-Trapped Excitons in Semiconductor Nanocrystals. *J. Phys. Chem. C* **2014**, *118*, 7730–7739.

49. Cihan, A. F.; Kelestemur, Y.; Guzelturk, B.; Yerli, O.; Kurum, U.; Yaglioglu, H. G.; Elmali, A.; Demir, H. V. Attractive versus Repulsive Excitonic Interactions of Colloidal Quantum Dots Control Blue- to Red-Shifting (and Non-Shifting)

Amplified Spontaneous Emission. *J. Phys. Chem. Lett.* **2013**, *4*, 4146–4152.

50. Kelestemur, Y.; Cihan, A. F.; Guzelturk, B.; Demir, H. V. Type-Tunable Amplified Spontaneous Emission from Core-Seeded CdSe/CdS Nanorods Controlled by Exciton-Exciton Interaction. *Nanoscale* **2014**, *6*, 8509–8514.

51. Guzelturk, B.; Kelestemur, Y.; Akgul, M. Z.; Sharma, V. K.; Demir, H. V. Ultralow Threshold One-Photon- and Two-Photon-Pumped Optical Gain Media of Blue-Emitting Colloidal Quantum Dot Films. *J. Phys. Chem. Lett.* **2014**, *5*, 2214–2218.

52. Xing, G.; Liao, Y.; Wu, X.; Chakrabortty, S.; Liu, X.; Yeow, E. K. L.; Chan, Y.; Sum, T. C. Ultralow-Threshold Two-Photon Pumped Amplified Spontaneous Emission and Lasing from Seeded CdSe/CdS Nanorod Heterostructures. *ACS Nano* **2012**, *6*, 10835–10844.

53. Raymond, J. E.; Bhaskar, A.; Goodson, T.; Makiuchi, N.; Ogawa, K.; Kobuke, Y. Synthesis and Two-Photon Absorption Enhancement of Porphyrin Macrocycles. *J. Am. Chem. Soc.* **2008**, *130*, 17212–17213.